Optimal Design of Kinematics Parallel Manipulator Considering Workspace and Control Effort

Diego A. Nunez, Mauricio Mauledoux, Oscar Aviles, Juan Guacheta, and Sebastian Gonzalez
Universidad Militar Nueva Granada, Ingenieria Mecatronica, Bogota, Colombia
Email: u7700100@unimilitar.edu.co, {mauricio.mauledoux, oscar.aviles, u1802715, est.sebastian.gonz1}@unimilitar.edu.co

***Abstract*—Several studies have reported the design of kinematics parallel mechanisms based on behavioral features; however, the design of this kind of system with six degrees of freedom considering parallelly volumetric behavior together with control effort remains to be accomplished. This work addresses the design of one type of these mechanisms based on two aspects: workspace and control effort. All aspects are considering and optimizing simultaneously through a multi-objective optimization technique based on a bio-inspired algorithm named Elitist Non-Dominated Sorting Differential Evolution Algorithm, which brings about a Pareto front. The workspace is determined using the inverse kinematics constrained boundaries analysis and a mono-objective optimization method. On the other hand, control effort is resolved by calculating the Euclidian norm of each torque signal of the system, which is controlled by a hybrid technique consisting of sliding modes and differential flatness. Finally, relations between the two studied aspects are depicted and analyzed.**

***Index Terms*—KINEMATICS parallel mechanism, HEXA, 6 dof, workspace, control effort, multi-objective optimization, differential evolution, pareto front**

I. Introduction

Among multidirectional options are robotic arms and Kinematics Parallel Mechanisms (KPMs). KPMs have many advantages compared to serial manipulators. The most relevant ones are the reduction of mechanical structure requirements, high rigidity, inertial response, precision, reduction of friction and noise, elimination of backslash, and fast response [1], [2]; all of them due to motors are fixed into the base. Nevertheless, the analysis of their dynamics is complex, and their workspace (WS) is smaller than their serial arm counterpart due to the ubication of motors causes interferences between each individual workspace of each arm [3]. Additionally, the parallel concept requires that inertial variations and mechanical coupling be reflected on the actuator axis which demands greater control effort (CE) and robust control strategies [4].

The WS and CE have reciprocal increment. While longer the links the greater WE and CE. Nevertheless, although a greater WS implies more volume capacity, high value of CE is related to higher energy consumption and issues with mechanical responses. Thus, it is necessary design KPMs considering these features simultaneously using multi-objective optimization techniques.

There are many applications of optimization techniques focused on parallel PKMs for instance trajectory path generation [5], topological configurations [6], and components design [7]. For this, in some cases have used bioinspired algorithms such as bee colony [8], particle swarm [9], genetic algorithms [10], cuckoo search [11], and differential evolution (DE) [12]. Each one offers advantages and disadvantages related to their Pareto front generation such as convergence, computing time, spread, among others [13]. For this study ED has been choice for its lower computational cost and faster convergence.

On the other hand, there are KPMs with kinematics chains compound of rotational, universal, and spherical joints (RUS) that have advantages related to the low weight of mobile parts, thinner rods that reduce collisions, cheaper components, and response time [14]. One of the most popular RUS manipulators is the six degrees of freedom HEXA manipulator type (6 RUS HEXA) (Fig. 1) that consists of six parallel extremities linked to a fixed platform at the upper and a mobile platform at the end of extremities depicted in Fig. 2.

Considering the advantages of 6 RUS HEXA and its design challenges related to WS and CE, the main contribution of this work is to present a multi-objective optimization strategy of dimensional parameters that minimize CE and maximize WS, which is solved by DE obtaining satisfactory results.

II. Methodology

The main was to determine the length of arm and rod links which directly affect the WS and CE. The methodology to reach the optimal design consisted of four steps. First, the determination of WS considered mechanical constraints.

Second, one figured out an index that quantified the CE. Third, one described WS and CE as objective functions implemented in a kind of DE multi-objective algorithm. Finally, a Pareto front was generated, and optimal points were studied.

Manuscript received October 12, 2021; revised January 21, 2022.

doi: 10.18178/ijmerr.11.4.234-240

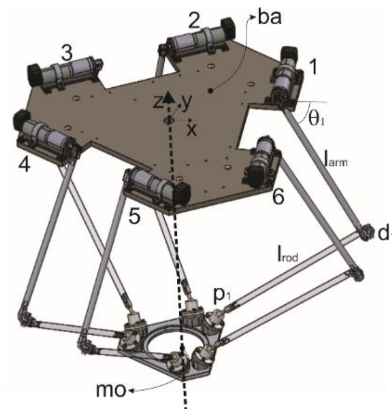

Figure 1. Hexa parallel mechanism.

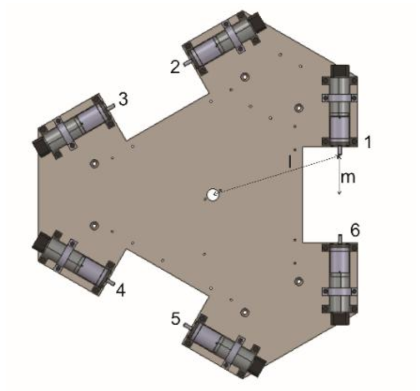

A.

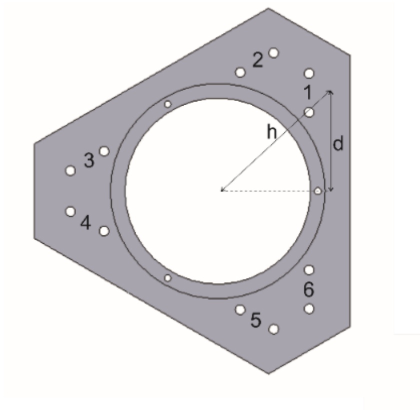

B.

Figure 2. Hexa platforms geometry. A. Fixed platforms. B. Mobile platform.

A. Workspace Determination

The WS is the volume where the KPM can move without mechanical constraints; usually, the WS is figured out by computing the inverse kinematics of each point; nevertheless, this method is computationally expensive. Therefore, Fig. 3 depicts another alternative to figure out the WS, which consisted in the determination of the boundary of movements to find the middle center point of a spherical cloud of points (which describe a position)[15] that was evaluated with the Golden Section Method to find limits position without restrictions. This method is explained below.

1) Description of fixed and mobile platform measurements

Fig. 1 describes the distribution of each ith corner of fixed and mobile platforms and the distribution of each ith arm. Next, from (1) to (12) are posing the geometrical description of platforms, where ba_i is the coordinate of the ith corner of the fixed platform, and mo_i is the coordinate of the ith corner of the mobile platform.

$$ba_1 = \left[l\, cos\left(asin\left(\frac{m}{l}\right)\right), \quad m, \quad 0 \right]^T \tag{1}$$

$$ba_6 = \left[l\, cos\left(asin\left(\frac{m}{l}\right)\right), \quad -m, \quad 0 \right]^T \tag{2}$$

$$ba_2 = Rotz\ (120°)\ ba_6 \tag{3}$$

$$ba_3 = Rotz\ (120°)\ ba_1 \tag{4}$$

$$ba_4 = Rotz(120°)\ ba_2 \tag{5}$$

$$ba_5 = Rotz\ (120°)\ ba_3 \tag{6}$$

$$mo_1 = \left[h\, cos\left(asin\left(\frac{d}{h}\right)\right), \quad d, \quad 0 \right]^T \tag{7}$$

$$mo_6 = \left[h\, cos\left(asin\left(\frac{d}{h}\right)\right), \quad -d, \quad 0 \right]^T \tag{8}$$

$$mo_2 = Rotz(120°)mo_6 \tag{9}$$

$$mo_3 = Rotz(120°)mo_1 \tag{10}$$

$$mo_4 = Rotz(120°)mo_2 \tag{11}$$

$$mo_5 = Rotz(120°)mo_3 \tag{12}$$

where,

$$Rotz(A) = \begin{bmatrix} cos(A) & -sin(A) & 0 \\ sin(A) & cos(A) & 0 \\ 0 & 0 & 1 \end{bmatrix}$$

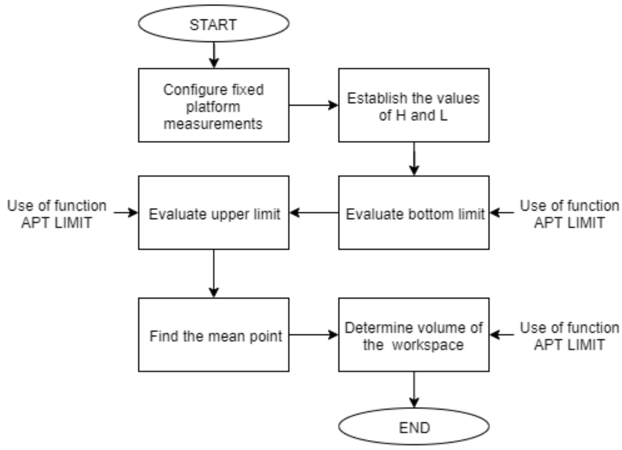

Figure 3. Flow chart of workspace determination.

2) Evaluation of bottom and upper limits

This step aimed to evaluate the limits of permitted movement of the mobile platform in the Z-axis, which was aligned with the center of the fixed platform (Fig. 1). The mobile platform movements in the Y and X-axis and rotations were equaled to zero. Determination of bottom and upper limits needed a function called APT LIMIT, which analyzed two coordinates to determine a vector between them. By the Golden Section optimization method, the magnitude of the vector where the constraint limits exist contemplating an adjust error was determined. Pseudocode 1 and Fig. 4.A describe the method mentioned above. In step 13, there is the function named EVAL POS; this function assessed the ability to reach a position with L_{arm} and L_{rod}; if the mechanism can reach that position, the function would respond TRUE otherwise FALSE. From (13) to (22), describe the calculation required to determine the feasibility to reach that position. Function EVAL POS was based on the value of the angle θ_i corresponding to ith arm, which determined with the inverse kinematics of the mechanism. If any θ_i is mechanically incongruous, the mechanism could not reach that position, and the function responsed FALSE.

Determination of θ_i was based on inverse kinematics and the relation of (13) of each ith open chain. Due to x_{d_i} depended on θ_i, that angle could be determined following (14).

$$L_{rod_i}{}^2 = \left(x_{d_i} - x_{Pi_i}\right)^2 + \left(y_{d_i} - y_{Pi_i}\right)^2 + \left(z_{d_i} - z_{Pi_i}\right)^2 \tag{13}$$

$$\theta(i) = atan\left(\frac{\frac{a\,c + b\delta}{b^2 + c^2}}{\frac{a\,b - c\delta}{b^2 + c^2}}\right) \tag{14}$$

$$\delta = \sqrt{(b^2 + c^2 - a^2)} \tag{15}$$

$$Pi = Rotx(\alpha)\ Roty(\beta)\ Rotz(\gamma)\ mo_i + \ Position\ evaluated \tag{16}$$

If i=1

$$\begin{aligned} a &= -\left(L_{arm}{}^2 - L_{rod}{}^2 - 0.15Pi_{i,2} - 0.43 * Pi_{i,1} + Pi_{i,1}{}^2 + Pi_{i,2}{}^2 + Pi_{i,3}{}^2 + 0.053\right) \\ b &= 0.43L_{arm} - 2L_{arm}Pi_{i,1} \\ c &= 2L_{arm}Pi_{i,3} \end{aligned} \tag{17}$$

If i=2

$$\begin{aligned} a &= -\left(L_{arm}{}^2 - L_{rod}{}^2 + Pi_{i,1}{}^2 + Pi_{i,2}{}^2 + Pi_{i,3}{}^2 + 0.09 * Pi_{i,1} - 0.45Pi_{i,2} + 0.053\right) \\ b &= 0.43L_{arm} + L_{arm}Pi_{i,1} - 1.73L_{arm}Pi_{i,2} \\ c &= 2L_{arm}Pi_{i,3} \end{aligned} \tag{18}$$

If i= 3

$$\begin{aligned} a &= -\left(L_{arm}{}^2 - L_{rod}{}^2 + Pi_{i,1}{}^2 + Pi_{i,2}{}^2 + Pi_{i,3}{}^2 + 0.34 * Pi_{i,1} - 0.303Pi_{i,2} + 0.053\right) \\ b &= 0.43L_{arm} + L_{arm}Pi_{i,1} - 1.73L_{arm}Pi_{i,2} \\ c &= 2L_{arm}Pi_{i,3} \end{aligned} \tag{19}$$

PSEUDOCODE I. APT LIMIT

Analysis by Golden Section of two points (ψ, ς) and determination of the coordinate where the constraint limit exists contemplating an adjust error.

```
1:   error value
2:   τ = ψ − ς
3:   mV = ||τ||                                   Magnitude of τ
4:   vup = û(τ)                                   Unitary vector of τ
5:   a = 0; b = mV
6:   Initializing: aw = 0; bw = 1; Lw = bw − aw; k = 0
7:   if |Lw (b − a)| > error
8:         while |Lw (b − a)| > error
9:             w1 = aw + 0.618 Lw
10:            w2 = bw − 0.618 Lw
11:            X1 = w1(b − a) + a
12:            PX1 = [X1vup + ς, 0,0,0]
13:                If EVAL POS in (PX1, L_arm, L_rod) = false
14:                 bw = w1
15:                else
16:                 aw = w2
17:                end if
18:            Lw = bw − aw
19:        end while
20:      Coordinate = PX1
21:  else
22:      w1 = aw + 0.618 Lw
23:      w2 = bw − 0.618 Lw
24:      PX1 = [ς, 0,0,0]
25:          If Eval Pos in (PX1, L_arm, L_rod) = false
26:             bw = w1
27:          else
28:             aw = w2
29:          end if
30:      Lw = bw − aw
31:      Coordinate = PX1
32:  end if
```

If i= 4

$$\begin{aligned} a &= -\left(L_{arm}{}^2 - L_{rod}{}^2 + Pi_{i,1}{}^2 + Pi_{i,2}{}^2 + Pi_{i,3}{}^2 + 0.34 * Pi_{i,1} + 0.303Pi_{i,2} + 0.053\right) \\ b &= 0.43L_{arm} + L_{arm}Pi_{i,1} + 1.73L_{arm}Pi_{i,2} \\ c &= 2L_{arm}Pi_{i,3} \end{aligned} \tag{20}$$

If i=5

$$\begin{aligned} a &= -\left(L_{arm}{}^2 - L_{rod}{}^2 + Pi_{i,1}{}^2 + Pi_{i,2}{}^2 + Pi_{i,3}{}^2 + 0.09 * Pi_{i,1} + 0.45Pi_{i,2} + 0.053\right) \\ b &= 0.43L_{arm} + L_{arm}Pi_{i,1} + 1.73L_{arm}Pi_{i,2} \\ c &= 2L_{arm}Pi_{i,3} \end{aligned} \tag{21}$$

If i= 6

$$\begin{aligned} a &= -\left(L_{arm}{}^2 - L_{rod}{}^2 + Pi_{i,1}{}^2 + Pi_{i,2}{}^2 + Pi_{i,3}{}^2 - 0.43 * Pi_{i,1} + 0.148Pi_{i,2} + 0.053\right) \\ b &= 0.43L_{arm} - 2L_{arm}Pi_{i,1} \\ c &= 2L_{arm}Pi_{i,3} \end{aligned} \tag{22}$$

where,

$$Rotx(\xi) = \begin{bmatrix} 1 & 0 & 0 \\ 0 & cos(\xi) & -sin(\xi) \\ 0 & sin(\xi) & cos(\xi) \end{bmatrix}$$

Once the APT LIMIT and EVAL POS functions have been described, the following step was to determine the bottom limit. First, was necessary a magnitude R (23) and an initial bottom coordinate in Z axis named γ (24).

$$R = 1.5\ (H + L) \tag{23}$$

$$\gamma = [0, 0, -R] \tag{24}$$

Determination of initial point (ς) is (25).

$$\varsigma = [0, 0, 0] \tag{25}$$

The bottom limit was also the application of function APT LIMIT evaluating γ and ς (26).

$$\text{Bottom Limit} = \text{APT LIMIT of } (\gamma, \varsigma) \tag{26}$$

Afterward, for determining the upper limit, it was necessary to establish a new coordinate ϑ for analyzing (27).

$$\vartheta = \left[0, 0, \frac{-R}{12}\right] \tag{27}$$

Once again, the initial point (ς) was (25). Once again, the upper limit was applying function APT LIMIT evaluating on ϑ and ς (28).

$$\text{Upper Limit} = \text{APT LIMIT } (\vartheta, \varsigma) \tag{28}$$

Next, the mean point or central point σ was figured out (29).

$$\sigma = \frac{\text{Upper Limit} + \text{Bottom Limit}}{2} \tag{29}$$

3) Workspace volume determination

Once the bottom, upper, and mean points were determined, the next step was to create a cloud of points distributed in the boundaries of the reachable space Fig. 4 B.

It was necessary to work with spherical coordinates because all points were described have a relation with a common center; this center point was the mean point above calculated. Spherical coordinates of points required a radio r, θ_j and ϕ_j angles and the central point σ (29), as shown (30) to (32).

$$x_{i,j} = R\sin(\theta_i)\cos(\phi_j) + \sigma_x \tag{30}$$

$$y_{i,j} = R\sin(\theta_i)\sin(\phi_j) + \sigma_y \tag{31}$$

$$z_{i,j} = R\cos(\theta_i)\sin(\phi_j) + \sigma_z \tag{32}$$

Initially, r was higher for assuring that the sphere encompasses all the future workspace volume. In that case $r = 1.5\,\|\text{Upper Limit} - \sigma\|$. Each point of the cloud points was created varying θ between 0 and 180 °ith steps and ϕ between -60 ° and 60 ° jth steps, ϕ has this interval because the mechanism was symmetric each 120 °. Thus, there was a vector formed by x, y, z, and σ. That vector was analyzed with function APT LIMIT (Pseudocode 1) for finding its highest magnitude without movement restriction and figure out the available coordinate η (33) (Fig. 4.B and Fig. 4. C). As a result, all points generated the boundary of the workspace.

$$\eta = \text{APT LIMIT } ([x, y, z], \sigma) \tag{33}$$

Finally, three closer points were selected from the cloud, and the area (χ) which they form was calculated (Fig. 4.D), then, the center point of the area χ was figured out, and the distance between this point and the center of the spherical coordinates (σ) was calculated. Hence the volume (Ξ) formed by those points could be evaluated. This process was repeated with all points, and the workspace of the mechanism was the sum of each volume Ξ (Fig. 4.E).

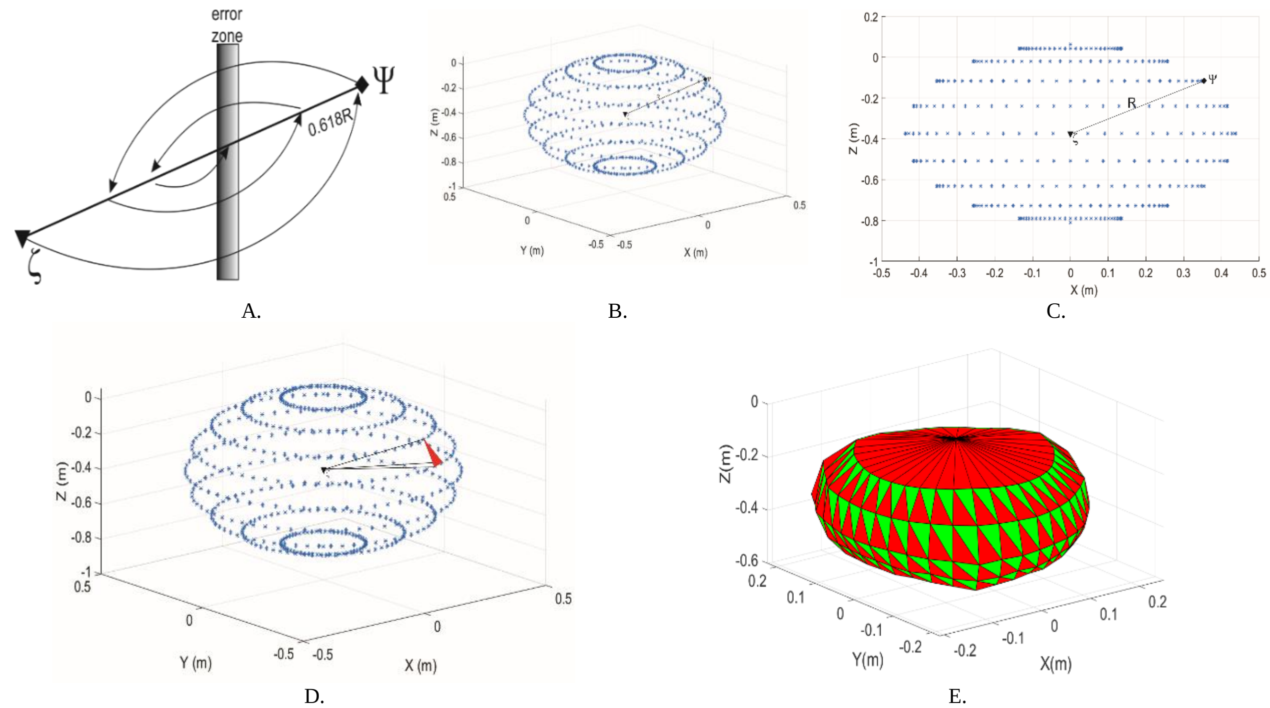

Figure 4. Schematic of WS obtention. A. Golden Section Searching Algorithm. B. Initial cloud of points. C. Vector place for evaluating position. D. Schematic of the area between 3 boundary points without constraints. E. Workspace of HEXA

B. Control Effort

Regarding 6 RUS HEXA, a Multi Input Multi Output system, the control strategy selected was a hybrid between sliding modes and differential flatness because it guarantees robustness against disturbances and unpredictable parameter variations of non-linear models. Fig. 5 depicts the configuration of the controller and mechanism; this configuration was composed of three subgroups: the Reference block, the Controller block, and the KPM block.

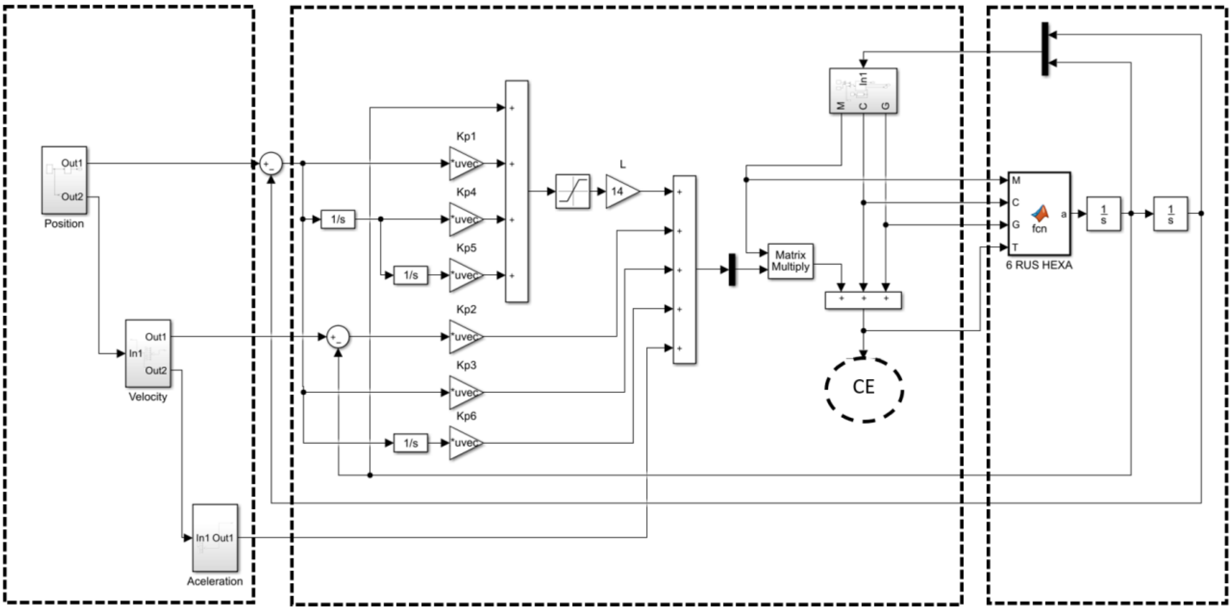

Figure 5. Diagram of KPM controlled by sliding modes and differential flatness control strategy.

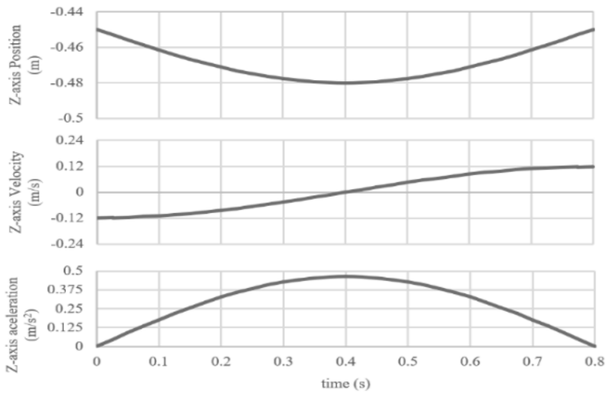

Figure 6. Position, velocity, and acceleration reference of Z-axis.

Position, velocity, and acceleration were simulated and configurated in the Reference block. Regarding position, a sine signal (Fig. 6) was applied in Z-axis, and the rest position equal zero. About velocity, the Z-axis position signal was derived and followed the same axis; similarly, the acceleration signal was derived from velocity.

The controller block consisted of the six controller parameters, which guaranteed 0.6 settling time and 0.7 damping ratio. Moreover, since the controller had a sliding mode section, it contained a switching function. Additionally, the dynamics modeling was determined by the Virtual Work and D'Alembert principle, which set the Inertial, Coriolis, and Gravity expressions. Finally, the controller provided a torque signal to the 6 HEXA RUS mechanism. From this signal, CE was determined. CE quantifies the energy-related to control the system, and it is the norm of each torque control signal. Therefore, CE is a scalar, and it depends on many aspects such as dimensions, time, control parameters, and the reference signal.

In the KPM block, there were the 6 RUS HEXA which was controlled by torque signal. The velocity and position were calculated, and there were used to feedback the control system.

C. *Multi-objective Optimization*

Above was mentioned that the aim was to determine the length of arms and rods considering a high WS and a low CE; those were the objective functions of the optimization algorithm. Multi-objective optimization was developed based on the Differential Evolution algorithm [16] and called Elitist Non-Dominated Sorting Differential Evolution (ENDSDE). This algorithm did not use a penalty function because kinematics analysis in the dynamical model contemplated the geometrical constraints. Pseudocode 2 describes ENDSDE with its respective subfunctions. Lines 1 and 2 determine the population size and number of parameters. Line 3 set Cr and F, which control the amplification of differential variations and crossover factor, respectively. Line 6 depicts the objective functions depending on the population. The Non-Dominated Sorting of line 12 followed the Naive and Slow approach [16]. ENDSDE stopped according to the number of times established by the convergence of results.

III. RESULTS

The simulation was a multi-objective optimization that analyzed and reached optimal length of arms and rods of 6 RUS HEXA simultaneously, performing using MATLAB and ENDSDE. ENDSDE delivered a set of optimal solutions that correspond to the Pareto front. This set was used to design optimal configuration.

After some preliminary simulations, the parameters showed in Table I were used in ENDSDE.

TABLE I. PARAMETERS USED FOR SIMULATING.

Population size	160
Parameters	(L_{arm}, L_{rod})
Upper and lower limits of parameters (m)	[0.3 , 0.5]
Generations	16
Cr	0.15
F $\left(\frac{2/npop+1.2}{2}\right)$	0.6

Fig. 7 depicts the distribution of those possible configurations in the function objective space.

Four of them were selected from the 160 solutions, and Table II presents their corresponding parameters and objective functions values.

TABLE II. PARETO FRONT. DECISION AND CRITERION SPACE

	L_{arm}	L_{rod}	WS	CE
f_1	0.3	0.5	3.0301	11.6872
f_2	0.399	0.499	4.4270	50.2205
f_3	0.459	0.499	5.4076	90.0519
f_4	0.5	0.5	5.8229	138.0332

Fig. 7 shows that two indexes conflicted. The CE increases when WS increase. For instance, a higher WS implies longer links which require more energy to move them; therefore, the use of intermediate solutions of Pareto front is recommended. Additionally, there were fewer available geometrical options at lower CE values, so that kind of arm-rod ratio presents more kinematics issues.

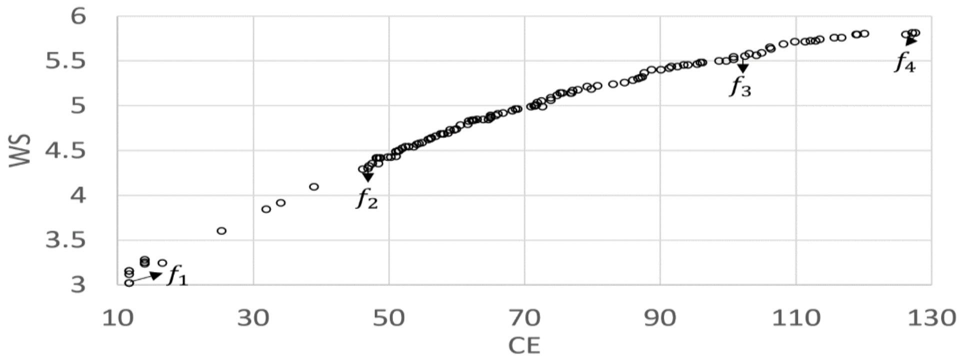

Figure 7. Pareto front of functions Worspace (WS) and Control Effort (CE).

IV. CONCLUSIONS

This work presents a computational method to calculate the WS of a KPM called 6 RUS HEXA based on mono-objective optimization and inverse kinematics analysis. Besides, one presents an index for quantifying the control energy consumption denominated CE. This measurement is the norm of the six signals of torque control signals through time simulation. In an ideal scenario, a KPM has a higher WS and a lower CE. In addition, one introduces a design procedure to reach geometrical parameters reflected in the lengths of arms and rods, optimizing WS and CE. Optimization design of this kind of KPM is a complex procedure because there is a contradictory objective function that must be satisfied.

Hence, the optimization algorithm must be robust and computationally efficient due to it needs to simulate many scenarios and configurations. ENDSDE showed a good performance, reached those optimal parameters, and provided a Pareto front of the possible set of solutions.

Future work will consider kinematics and dynamics behavior such as Global Conditioning Index, Global Gradient index, Global Conditioning Dynamical Index, actuator limits, control parameters, stiffness of links, and even different control methodologies.

PSEUDOCODE 2. MULTI-OBJECTIVE OPTIMIZATION

Set population size →npop.
Parameters →nparam
Determination of Cr *and* F
where,
$Cr \in [0 , 1]$ $F \in [0 , 2]$
Upper and lower limits of parameters → $X_{u,l}$: $(L_{arm_{u,l}}, L_{rod_{u,l}})$
Create initial parents→$P^{(0)}$: $rand(X_u - X_l) + X_l \cup X_{u,l}$
where,
$rand \in [0 , 1]$
$[EC_{P^{(0)}} , WS_{P^{(0)}}] : f(P^{(0)})$
for j=1…npop and i=1, …, nparam
$P^{G+1}{}_{i,j} : \begin{cases} P^{(G)}{}_{c,i,j} + F\left(P^{(G)}{}_{A,j} - P^{(G)}{}_{B,j}\right) & if\ rand \le Cr\ or\ j \\ P^{(G)}{}_{j} & otherwise \end{cases}$
where,
A: 1, …, npop *B: 1, …, npop* *C: 1, …, npop*
D: 1, …, nparam $A \neq B \neq C$
$[EC_{G+1,j} , WS_{G+1,j}] : f(X^{G+1}{}_j)$
end for
$R_t = P^{(0)} \cup P^{G+1}$
Non-Dominated Sorting of R_t.
$[EC_{R_t} , WS_{R_t}] : f(R_t) : M$
Set new population $P_{t+1} = 0$. $Set\ i = i + 1$
Identify different fronts $(\mathcal{F}_i)$
Crowding-sort
While size of M <= npop
Assign $d_i=0$
Find de maximum and minimum value of M f^{max}, f^{min}
Determine the distance (d) between near points of m. $m \in M$
$d = d_m + \left|\frac{f^{i+1}_{(m)} - f^{i-1}_{(m)}}{f^{max} - f^{min}}\right|$
end while
Divide M into subgroups depending of $\mathcal{F}$
Sort each subgroup of M in descending order according to d
Parameters of M (X^M) *are the new Parents→*P^{++}
Create new offsprings G^{++} *from* P^{++}

CONFLICT OF INTEREST

The authors declare no conflict of interest.

AKNOWLEDGMENT

This work was supported by Vicerrectoría de Investigaciones, Universidad Militar Nueva Granada trought project IMP ING 3122, "Desarrollo de un sistema optimo de deposición de material para un mecanismo de cinemática paralela de seis grados de libertad enfocado en manufactura aditiva". Este estudio fue realizado y soportado gracias a la Vicerrectoría de Investigaciones de la Universidad Militar Nueva Granada a través del proyecto IMP ING 3122 titulado "Desarrollo de un sistema óptimo de deposición de material para un mecanismo de cinemática paralela de seis grados de libertad enfocado en manufactura aditiva".

REFERENCES

[1] Z. F. Shao, X. Tang, X. Chen, and L. P. Wang, "Research on the inertia matching of the Stewart parallel manipulator," *Robot. Comput. Integr. Manuf.*, vol. 28, no. 6, pp. 649–659, 2012.

[2] P. Ogbobe, Z. Ye, H. Jiang, and J. Han, "Analytical formulation of coupling effects matrix between degrees of freedom motion of parallel robots," in *Proc. 2010 International Conference on Intelligent Computation Technology and Automation (ICICTA)*, vol. 1, 2010, pp. 711–714.

[3] S. N. Nabavi, A. Akbarzadeh, and J. Enferadi, "A study on kinematics and workspace determination of a general 6-PUS robot," *J. Intell. Robot. Syst. Theory Appl.*, vol. 91, no. 3–4, pp. 351–362.

[4] A. Valencia, M. Mauledoux, and C. Castañeda, "Design of dynamic controllers for continuous paths on parallel platforms (Slide Modes and PD+)," *MATEC Web Conf.*, vol. 306, no. 20 20, p. 03005, 2020.

[5] C. Choubey and J. Ohri, "Optimal trajectory generation for a 6-DOF parallel manipulator using grey wolf optimization algorithm," *Robotica*, vol. 39, no. 3, pp. 411–427, March 2021.

[6] J. You, F. Xi, H. Shen, J. Wang, and X. Yang, "A novel Stewart-type parallel mechanism with topological reconfiguration: Design, kinematics and stiffness evaluation," *Mech. Mach. Theory*, vol. 162, p. 104329, Aug. 2021.

[7] X. Du, Y. Li, P. Wang, Z. Ma, D. Li, and C. Wu, "Design and optimization of solar tracker with U-PRU-PUS parallel mechanism," *Mech. Mach. Theory*, vol. 155, p. 104107, Jan. 2021.

[8] S. Dereli and R. Köker, "Simulation based calculation of the inverse kinematics solution of 7-DOF robot manipulator using artificial bee colony algorithm," *SN Appl. Sci. 2019 21*, vol. 2, no. 1, pp. 1–11, Dec. 2019.

[9] S. Zhang, X. Yuan, P. D. Docherty, K. Yang, and C. Li, "An improved particle swarm optimization algorithm and its application in solving forward kinematics of a 3-DoF parallel manipulator," in *Proc. Inst. Mech. Eng. Part C J. Mech. Eng. Sci.*, vol. 235, no. 5, pp. 896–907, July 2020.

[10] A. Rosyid, B. El-Khasawneh, and A. Alazzam, "Genetic and hybrid algorithms for optimization of non-singular 3PRR planar parallel kinematics mechanism for machining application," *Robotica*, vol. 36, no. 6, pp. 839–864, June 2018.

[11] S. Panda, D. Mishra, and B. B. Biswal, "An approach for design optimization of 3R manipulator using adaptive cuckoo search algorithm," *https://doi.org/10.1080/15397734.2019.1675166*, vol. 48, no. 6, pp. 773–798, Nov. 2019.

[12] M. G. Villarreal-Cervantes, "Approximate and widespread pareto solutions in the structure-control design of mechatronic systems," *J. Optim. Theory Appl.*, vol. 173, no. 2, pp. 628–657, May 2017.

[13] V. D. Coello, Carlos, Lamont Gary, *Evolutionary Algorithms for Solving Multi-Objective Problems*, 2nd ed. 2007.

[14] E. C. Castaneda, R. R. Alvarado, J. C. Koo, and E. C. Castañeda, "Optimum design of the reconfiguration system for a 6-degree-of-freedom parallel manipulator via motion/force transmission analysis optimum design of the reconfiguration system for a 6-degree-of-freedom parallel manipulator via motion/force transmission analysis," *Artic. J. Mech. Sci. Technol.*, vol. 34, no. 3, p. 2020, 2020.

[15] S. T. Filho and E. Cabral, "Kinematics and workspace analysis of a parallel architecture robot: the Hexa," in *Proc. 18th Int. Congr. Mech. Eng. Novemb. 6-11, Ouro Preto, MG*, vol. 2, no. August, pp. 158–165, 2005, [Online]. Available: http://www.abcm.org.br/pt/wp-content/anais/cobem/2005/PDF/COBEM2005-0095.pdf.

[16] K. Deb, *Optimization for Engineering Design*, 2nd ed. New Delhi: PHI Learning Private Limited, 2012.

Diego A Nunez received his B.S. in mechatronics engineering from Universidad Militar Nueva Granada in 2005 and his M.Sc in mechanical engineering from Universidad de Los Andes in 2014. He is a specialist in Polymer Processing and currently, he is working toward a Ph.D. degree in Applied Science at Universidad Militar Nueva Granada. His research interests include parallel robots, optimization, additive manufacturing, and mechanical behavior of materials.

Mauricio Mauledoux received his B.S. in mechatronics engineering from Universidad Militar Nueva Granada in 2005. In 2011 He received his Ph.D. degree in mathematical models, numerical methods and software systems (Red Diploma) from St. Petersburg State Polytechnic University, Russia. In 2012, he joined the Department of Mechatronics Engineering, at Universidad Militar Nueva Granada in Colombia as Assistant Professor. His current research interests include robotics, automatic control, multi-agent systems, smart grids, and optimization

Oscar Aviles is an electronics engineer from Universidad Antonio Nariño in Bogota, 1995. In 2006, he received his M.Sc degree in production automatic systems at Universidad Tecnológica de Pereira and he received his Ph.D. degree in mechanical engineering at Universidade Estadual de Campinas in 2008. Currently, he is a professor of mechatronics engineering at Universidad Militar Nueva Granada, and his main research interests focused on biomechatronics, rehabilitation engineering, and robotics.

Juan Guacheta received his B.S. in mechatronics engineering from Universidad Militar Nueva Granada in 2020. Currently, he is working toward the M.Sc degree in mechatronics engineering at Universidad Militar Nueva Granada. His research interests include robotics, multi-agent systems and optimization.

Sebastian Gonzalez received the B.S. in mechatronics engineering from Universidad Militar Nueva Granada in 2020. Currently, he is working toward the M.Sc degree in Mechatronics Engineering at Universidad Militar Nueva Granada. His research interests include optimization, electronics and robotics.